


**Conformal Invariance in Water-Wave Turbulence**M. Nosedá<sup>✉\*</sup> and P. J. Cobelli<sup>✉†</sup>*Universidad de Buenos Aires, Facultad de Ciencias Exactas y Naturales,  
Departamento de Física, Ciudad Universitaria, 1428 Buenos Aires, Argentina  
and CONICET - Universidad de Buenos Aires, Instituto de Física Interdisciplinaria y Aplicada (INFINA),  
Ciudad Universitaria, 1428 Buenos Aires, Argentina* (Received 30 August 2023; accepted 25 January 2024; published 28 February 2024)

We experimentally investigate the statistics of zero-height isolines in gravity wave turbulence as physical candidates for conformal invariant curves. We present direct evidence that they can be described by the family of conformal invariant curves called stochastic Schramm-Löwner evolution (or  $SLE_\kappa$ ), with diffusivity  $\kappa = 2.88(8)$ . A higher nonlinearity in the height fields is shown destroy this symmetry, though scale invariance is retained.

DOI: [10.1103/PhysRevLett.132.094001](https://doi.org/10.1103/PhysRevLett.132.094001)

Symmetries in physics underpin fundamental laws and reveal profound connections between seemingly unrelated phenomena. Scale invariance, for instance, establishes links between disparate processes, ranging from phase transitions, galaxy clustering, and crack propagation to avalanches in granular media, and social networking. In certain systems exhibiting critical behavior, conformal invariance emerges as a broader symmetry in which the properties remain unaltered under conformal transformations, i.e., geometrical transformations that preserve angles and allow for nonuniform rescaling of distances.

Conformal symmetry plays a central role in understanding critical phenomena, scaling behaviors, and emergent properties across classical and quantum field theory domains—from particle physics to condensed matter, turbulence, and string theory [1,2]. In 2D, conformal invariance completely determines the scaling exponents and correlation functions of a wide class of theories at criticality [3], enabling a thorough classification of universality classes of critical phenomena.

In recent years, the discovery of Schramm-Löwner Evolution (SLE) has provided physicists with a powerful and versatile framework for the statistical characterization of conformal invariance in physical systems [4–7]. SLE is a class of non-self-intersecting random planar curves that can be mapped into a one-dimensional Brownian walk with diffusivity  $\kappa$ , and thus have conformal invariant statistics. Moreover,  $SLE_\kappa$  gives rise to a natural classification (by the value of  $\kappa$ ) of conformal curves in the plane, such as the boundaries of clusters in 2D critical processes described by conformal field theories.

Studies based on the SLE formalism have revealed surprising connections between diverse branches of physics. Pioneering research showed, for example, that the zero-vorticity lines in the inverse cascade of 2D Navier-Stokes turbulence are conformal invariant and statistically

equivalent to the boundaries of percolation clusters [8,9], whereas temperature isolines in surface quasigeostrophic turbulence were found to belong to the same universality class as domain walls in the  $O(2)$  spin model [10]. Conformal invariance was also reported for nodal lines of random wave functions [11,12], domain walls of spin glasses [13,14], rocky shorelines [15], isoheight lines on growing solid surfaces [16,17], avalanche frontiers in sandpile models [18], a class of active scalar turbulence [19], isovorticity lines in 3D rotating turbulence [20], watersheds dividing drainage basins [21], graphene sheets [22], and critical percolation clusters [23,24].

Turbulence is defined as the state of a physical system with many interacting degrees of freedom deviated far from equilibrium. The main fundamental inquiry in turbulence concerns the degree of universality and the symmetries of the turbulent state; particularly which symmetries remain broken and which ones are restored in the developed stage [25]. In this context, the aforementioned SLE-based studies demonstrated the emergence of conformal invariance in various dual cascade turbulent systems, all characterized by the prevalence of vortices [8,9,19,20]. Since wave turbulence systems are known to exhibit properties similar to those of their vortex counterparts (such as scale invariance, universality, and dual cascades), the question naturally arises: can conformal invariance be observed in wave turbulence scenarios, i.e., in turbulent systems dominated by the coupling between random nonlinear waves? This subject is particularly important for its potential implications, as wave turbulence is present in a vast range of physical processes and scales; from the ocean state to nonlinear optics, from quantum fluids to gravitational waves [26–29].

In this Letter, we address this question experimentally for the case of water-wave turbulence, a dual cascade system [26] theorized to present conformal invariance [3].

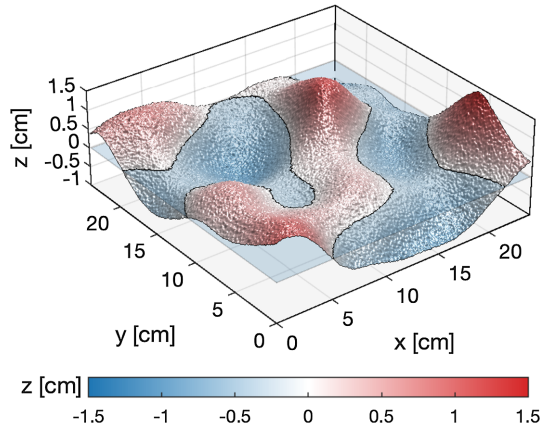


FIG. 1. Snapshot of the reconstructed height field  $h(x, y)$ . As a visual reference, the position of the free surface at rest (corresponding to  $z = 0$ ) is represented by a translucent blue plane. Zero-height isocontours of  $h(x, y)$  are depicted, onto the free surface, by solid black lines.

Our results show that the zero-height isolines of weak water-wave turbulence are, within experimental uncertainty, compatible with stochastic Schramm-Löwner evolutions, with statistics remarkably close to those of domain walls in the critical 2D Ising model [30].

In our experiments, water-wave turbulence is generated by the horizontal motion of two piston-type wave maker paddles (150 mm in width, 30 mm immersed) within a  $(1000 \times 800)$  mm<sup>2</sup> open-top PMMA transparent tank filled with the working fluid up to a rest height of 50 mm. The wave makers are independently controlled by two linear servomotors, with a positional repeatability of  $\pm 0.05$  mm and 44 N peak force. Their motion is subjected to a random forcing (both in amplitude and phase) with a white frequency spectrum bandpass-filtered in the 0–4 Hz range, with adjustable maximum amplitude. This forcing scheme is known to produce cascades of water-wave turbulence in laboratory experiments [31–34]. In this study, we investigated the effects of two peak forcing amplitudes: 5 mm (AMP5) and 10 mm (AMP10); the latter representing a fourfold increase in driving power relative to the former.

We employ diffusive light photography (DLP) to obtain 3D measurements of the topography of the wave field. This optical technique [35,36] allows us to measure the local free-surface height  $h(x, y, t)$  in a region of  $(241.5 \times 241.5)$  mm<sup>2</sup>. The surface dynamics is recorded by a high-speed camera with a resolution of  $(1024 \times 1024)$  px<sup>2</sup>, at 60 Hz and 1/3000 s shutter speed (for experimental details, see Supplemental Material, Sec. I [37], which includes Refs. [38–43]). Each experimental realization comprises 1700 consecutive frames, covering a duration of 28.3 s. Throughout our experimental campaign, each dataset consists in five independent realizations conducted under identical experimental conditions.

Figure 1 shows an example of free-surface reconstruction obtained by the DLP technique. Individual isocontours of

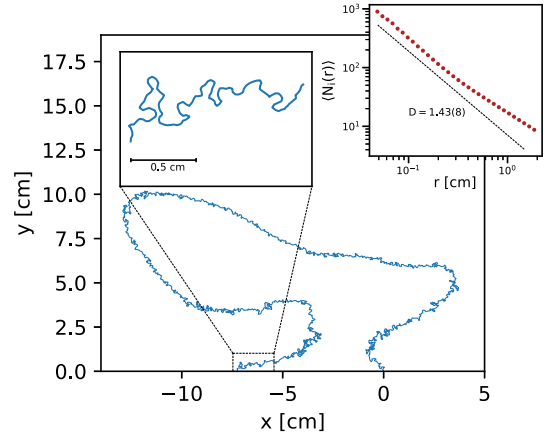


FIG. 2. Example candidate trace and fractal dimension estimation for the AMP5 dataset. A close-up view on the last points of the trace is presented in the left inset, highlighting the complex structures present at smaller scales. The right panel shows, for the AMP5 dataset, the power-law scaling of the (mean) number of sticks required for traveling the traces as a function of their length (circles).

zero height, depicted in the figure as black curves over the  $z = 0$  plane, are derived from the reconstructed fields using the *contour* function in MATPLOTLIB [44]. This function employs a marching squares algorithm and linear interpolation to define the isolines as a series of discrete points in the  $(x, y)$  plane. By construction, each contour line is oriented so that positive height sites are consistently positioned to its left.

From the complete set of zero-height isolines, candidate SLE traces are identified as follows. First, for each free-surface reconstruction, a horizontal line representing a real  $x$  axis in the complex plane is drawn across the height field. Any contiguous portion of a zero-height isoline that lies between two successive intersections with the real axis is considered a candidate trace. This process is repeated for all four possible orientations of each height map, corresponding to incremental rotations in steps of  $\pi/2$  radians.

To avoid using time-correlated paths, we only select candidate traces corresponding to height fields separated by  $n$  frames, using  $n = 10$  and only keeping traces that exceed lengths of  $l = 500$  points (larger values of both  $n$  and  $l$  yield similar results). Following this procedure, we collected a total of 1154 candidate traces for AMP5, with an average of 1908 points per trace. Similarly, AMP10 yielded 1337 putative traces, each consisting of an average of 1637 points.

Figure 2 shows an example candidate trace belonging to the AMP5 dataset. An initial observation reveals a rich and intricate structure, hinting at the existence of underlying complexity. Moreover, a close-up view on an arbitrarily chosen part of it (depicted in the upper-left inset) evinces the persistence of such structures across different scales, suggesting the presence of self-similarity or fractal-like characteristics.

In order to investigate the scaling behavior of the candidate traces we estimate their fractal dimension by means of Richardson's yardstick method [45]. In this method, a yardstick of length  $r$  is considered and the length of the candidate trace is defined by the number of straight yardsticks  $N(r)$  required to go from one extreme to the other by jumping from one point on the curve to the next at a distance  $r$ . The fractal (or capacity) dimension  $D_0$  is defined as the limit  $D_0 = -\lim_{r \rightarrow 0^+} \log N(r) / \log(r)$ . Prior to its application to candidate traces, we validated our implementation of the yardstick algorithm with synthetic traces [46,47] (for details, see Supplemental Material [37]).

For each candidate trace (indexed by  $i$ ),  $N_i(r)$  was computed across a scale range spanning the dataset minimum to maximum point separation. The ensemble average at a fixed scale, denoted as  $\langle N_i \rangle(r)$ , is presented in the top-right panel of Fig. 2 for the AMP5 dataset. A power-law relation is evident at small  $r$ , spanning a decade of scales within the available range. The best fit to the data (depicted as a dotted line), results in  $D_0 = 1.43 \pm 0.08$ . A similar analysis for the AMP10 dataset yields  $D_0 = 1.35 \pm 0.07$  (not shown). These results indicate that candidate traces exhibit statistical self-similarity across the resolved scales, providing strong support for scale invariance in our datasets; a necessary (though not sufficient) condition for conformal invariance.

To probe the conformal invariance of these curves, we consider a self-avoiding curve  $\gamma(t)$ , parametrized by the time  $t$ , which begins at the origin and extends to  $\infty$ . At any time  $t$ , the upper half-plane  $\mathbb{H}$  minus the curve up to that point, can be mapped back onto  $\mathbb{H}$  by an analytic function  $g_t(z)$ , made unique on imposing the asymptotic condition  $g_t(z) \sim z + 2t/z + O(1/z^2)$  for  $z \rightarrow \infty$ . The growing tip of the curve is therefore mapped to a point  $\xi(t)$  on the real axis. The curve  $\gamma(t)$  and the conformal map  $g_t(z)$  are completely parametrized by the driving function  $\xi(t)$ , and satisfy the chordal Löwner equation [48]:

$$\frac{dg_t}{dt} = \frac{2}{g_t(z) - \xi(t)}. \quad (1)$$

In the case of random curves, Eq. (1) is called Schramm-Löwner evolution (SLE), and the driving function is a random variable. Schramm demonstrated that the statistics of random curves are conformal invariant if and only if the driving function is a Brownian walk [49], i.e., a random function with uncorrelated increments and satisfying  $\sigma_\xi^2 = \langle [\xi(t) - \langle \xi(t) \rangle]^2 \rangle = \kappa t$ . Here,  $\kappa$  is the diffusivity which allows for the classification of the conformal invariant random curves into universality classes denoted by SLE $_\kappa$ .

Therefore, in order to test the conformal invariance of the zero-height isolines, it is necessary to assess whether their driving functions are statistically a Gaussian process, and specifically if it corresponds to Brownian motion (termed

direct test). If this were the case, the diffusivity  $\kappa$  should also be determined.

The first step consists in extracting the driving functions of our candidate SLE traces by inversion of the Löwner equation. As Eq. (1) is valid for chordal curves, the traces given by the set of points  $\{z_0, z_1, \dots, z_N\}$  are first translated to the origin and then mapped using a Möbius transformation of the form  $\varphi(z) = z_N z / (z_N - z)$ , to ensure that the curves start at the origin and end at infinity. We verified that this procedure does not modify our results greatly.

Assuming that the ensemble of zero-height isolines is statistically equivalent to SLE curves, we derived the associated driving functions ensemble using the zipper algorithm with vertical slits [50,51] (chosen among the many available numerical algorithms [52]). This algorithm is based on the solution of Eq. (1) for a simple trace made of an infinitesimal vertical line segment, given by  $g_{\xi_t, \delta t}(z) = \xi_t + \sqrt{(z - \xi_t)^2 + 4\delta t}$ . This conformal transformation maps the upper half-plane, excluding the vertical slit joining the points  $\xi_t$  and  $\xi_t + 2i\sqrt{\delta t}$ , back into the upper half-plane. The process begins with  $z_0 = (0, 0)$ , and all subsequent points except the first one are mapped by  $g_{\xi_t, \delta t}(z)$ , with  $\delta t = \frac{1}{4} \text{Im}(z_1)^2$  and  $\xi_t = \text{Re}(z_1)$ . The resulting set of points is renumbered, resulting in a curve one element shorter than the original. By repeating this procedure on the remaining points, the algorithm zips the entire trace onto the real axis by the composition of conformal maps. After mapping all points to the real axis, this results in a sequence of discrete Löwner times  $t_j$  and driving values  $\xi_{t_j}$  that approximate the true driving functions. Last, the final Löwner time for all traces is renormalized to 1, using the scaling property of SLE [53].

We begin by considering the AMP5 dataset. An ensemble average over the driving functions allows us to observe a linear growth of the variance  $\sigma_\xi^2 = \langle [\xi_t - \langle \xi_t \rangle]^2 \rangle$  with Löwner time, as shown in Fig. 3 (circles). To quantify this observation, we perform a fit of the form  $\sigma_\xi^2(t) = \kappa t^\alpha$  within that time range, represented by a solid line in the figure. Notably, our analysis confirms the initial observation, yielding a value of  $\alpha = (1.00 \pm 0.01)$ , providing strong support for the linear scaling hypothesis. Moreover, we find the best estimate for the diffusivity to be  $\kappa = (2.88 \pm 0.08)$ . The compensated value of the variance, i.e.,  $\sigma_\xi^2(t)/t \sim \kappa(t)$ , is shown in the upper-left inset of Fig. 3 in circles, along with the best estimate from the fit, represented by a solid line. A plateau that extends throughout the range of Löwner times is clearly observed.

In contrast, repeating this analysis with the AMP10 dataset yields qualitatively different results. In particular, for this dataset the variance of the driving functions does not scale linearly with Löwner time. This is evidenced by the lack of a plateau in the compensated variance for this dataset, represented by squares in the top-left inset of Fig. 3.

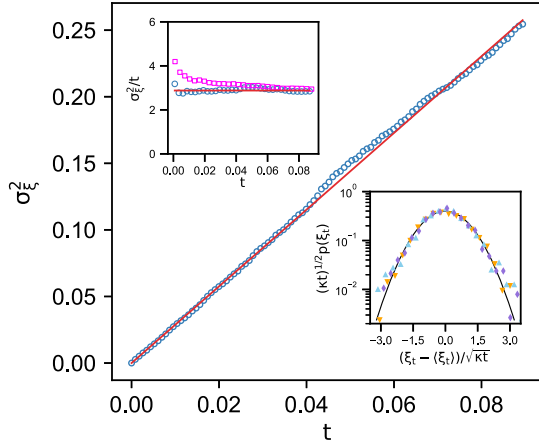


FIG. 3. Statistics of the ensemble of driving functions. Main frame: linear behavior of  $\sigma_{\xi}^2(t)$  for traces in the AMP5 dataset, with a slope of  $\kappa = 2.88(8)$ . Upper-left inset: diffusivity  $\kappa$ , in circles and squares for the AMP5 and AMP10 datasets, respectively. Lower-right inset: PDF of the rescaled driving functions for curves in the AMP5 dataset, at three different times:  $t = 0.0015$  (inverted triangles),  $0.045$  (triangles), and  $0.09$  (diamonds); the solid line represents a standard Gaussian distribution.

We associate this breakdown of conformal invariance to an increase in the level of nonlinearity in the interaction between waves. This becomes apparent when examining the typical root mean square wave steepness  $\sigma_s$ , defined as the standard deviation of the magnitude of the gradient of  $h$  [39]. Remarkably, the AMP10 dataset exhibits a  $\sigma_s$  value of 0.21, nearly double that of the AMP5 dataset, which is characterized by  $\sigma_s = 0.11$ . The heightened nonlinearity manifests also in the distribution of wave height values, with AMP10 displaying a greater departure from Gaussianity compared to AMP5 (see Supplemental Material, Sec. II [37]).

We proceed by testing whether  $\xi_t$  is a Gaussian process. We conducted Kolmogorov-Smirnov tests on the standardized driving  $[\xi_t - \langle \xi_t \rangle]/(\kappa t)^2$ , separately for each (discrete) Löwner time available within the range where linearity was established. The results indicate that, at a significance level of 0.05, the null hypothesis of Gaussianity is not rejected in any of the individual tests. Upon combining the  $p$  values from these multiple tests using Fisher's method, the combined  $p$  value of 0.78 does not provide sufficient evidence to reject the null hypothesis. This suggests that the driving process  $\xi_t$  appears consistent with a Gaussian distribution. Correspondingly, the probability density function (PDF) of the standardized driving collapses onto a standard Gaussian distribution, as illustrated in the lower-right inset of Fig. 3 for three Löwner times.

For conformal invariant traces, the fractal dimension and the diffusivity of the associated  $\text{SLE}_{\kappa}$  process are related by  $D_0 = \min\{2, 1 + \kappa/8\}$  [54]. As we have independently determined both  $D_0$  and  $\kappa$  for the zero-height isolines, this theoretical prediction serves as a consistency check for our

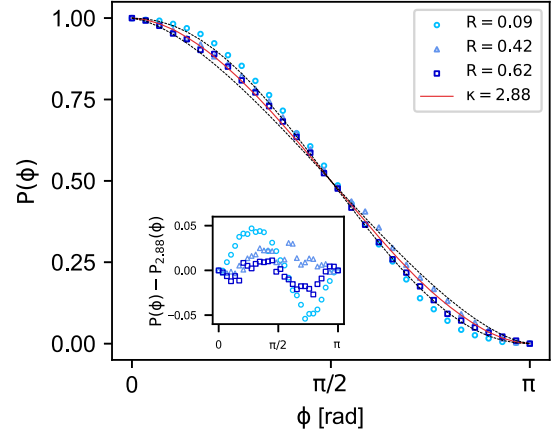


FIG. 4. Left passage probability  $P(\phi)$  for the zero-height isolines of wave turbulence, for different radii within the variance linear regime. The solid line corresponds to the theoretical prediction for  $\kappa = 2.88$ , the diffusivity value obtained by the direct test; dashed lines represent the edges of 10% envelopes around that value. The corresponding residuals  $P(\phi) - P_{2.88}(\phi)$ , are shown in the inset.

findings. Remarkably, the fractal dimension derived from that expression using  $\kappa = 2.88(8)$  yields a value of  $D_0^{(\kappa)} = (1.36 \pm 0.01)$ , in agreement with the one previously obtained.

We finally consider the left passage probability (LPP). This property quantifies the probability  $P_{\kappa}(\phi)$  of a chordal  $\text{SLE}_{\kappa}$  trace passing to the left of a given point  $Re^{i\phi}$  in  $\mathbb{H}$ , where  $R$  and  $\phi$  are the distance and the angle between the origin and the point. Because of scale invariance,  $P_{\kappa}(\phi)$  is independent of  $R$ , and SLE theory [49] predicts that

$$P_{\kappa}(\phi) = \frac{1}{2} + \frac{\Gamma(\frac{4}{\kappa})}{\sqrt{\pi}\Gamma(\frac{8-\kappa}{2\kappa})} {}_2F_1\left(\frac{1}{2}, \frac{4}{\kappa}; \frac{3}{2}, -\cot^2\phi\right) \cot(\phi), \quad (2)$$

where  ${}_2F_1$  and  $\Gamma$  represent the Gauss hypergeometric and Gamma functions, respectively. For this test, the traces are regenerated from their individual driving functions with the ensemble mean  $\langle \xi_t \rangle$  subtracted. The LPP is calculated as the (normalized) number of curves passing to the left of a point in the upper half-plane. Figure 4 presents the results for  $P(\phi)$  for traces in the AMP5 dataset. To assess its independence from radial distance, we systematically computed the LPP for different radii, three of which are shown in the figure. Those specific radii, chosen to illustrate the typical behavior observed for the LPP, correspond on average to Löwner times located at the initial, intermediate and final stages of the linear scaling regime shown in Fig. 3. The analytical prediction  $P_{2.88}(\phi)$  from Eq. (2) with  $\kappa = 2.88$  is depicted by a solid line, while dashed lines represent  $\pm 10\%$  of this value. The inset displays the residuals  $P(\phi) - P_{2.88}(\phi)$  for the radii considered in the main figure. Our results for the LPP exhibit good agreement with the theoretical prediction for  $\kappa = 2.88$ .

In summary, we presented an experimental study that shows compatibility between SLEs and zero-height isolines of water-wave turbulence. This argument is supported by four mutually independent standardized tests performed on our data, namely: linearity of the variance with Löwner time (direct SLE test), Gaussianity assessment through Kolmogorov-Smirnov testing, fractal dimension of the traces, and left passage probability. Within the AMP5 dataset, all tests are in agreement with SLE predictions, and lead to numerically consistent results for the diffusivity. In particular, our results yield  $\kappa = 2.88(8)$ , a value close to that of domain walls in the critical 2D Ising model, with  $\kappa = 3$  [30]. Although this cannot be interpreted as proof, the extension of theoretical prediction [3] with our experimental findings constitutes a robust indication for conformal invariance in the weakly coupled limit. In contrast, the AMP10 dataset, characterized by higher forcing, larger deviations from Gaussianity in the distribution of wave height, and heightened nonlinearity (as evidenced by its wave steepness), does not demonstrate compatibility with the SLE family (yet retains scale invariance).

The observation that the zero-height isolines are conformal invariant places the study of water-wave turbulence within the theory of critical phenomena, and suggests that at least part of its statistics could be described in terms of a conformal field theory. Finally, our results naturally bring forward the question as to whether other systems exhibiting wave turbulence may also present conformal invariance as a restored symmetry, and if so, to what universality classes would they belong. This can open a new approach to the general study of the broad class of nonlinearly interacting systems described by wave turbulence.

The authors acknowledge support from Grants Proyectos de Investigación Científica y Tecnológica No. 2018-4298, and UBACyT No. 20020170100508. Moreover, the authors are grateful to Pablo Mininni for fruitful discussions.

\*mnosed@df.uba.ar

†cobelli@df.uba.ar

- [1] C. Itzykson, H. Saleur, and J. Zuber, *Conformal Invariance and Applications to Statistical Mechanics* (World Scientific Publishing Company, Singapore, 1998).
- [2] M. Henkel, *Conformal Invariance and Critical Phenomena, Theoretical and Mathematical Physics* (Springer, Berlin, Heidelberg, 2013).
- [3] J. Cardy, G. Falkovich, K. Gawedzki, and O. V. Zaboronski, *Non-Equilibrium Statistical Mechanics and Turbulence*, 1st ed., edited by S. Nazarenko and O. V. Zaboronski, London Mathematical Society Lecture Note Series Vol. 355 (Cambridge University Press, Cambridge, 2008).
- [4] O. Schramm, *Isr. J. Math.* **118** (2000).
- [5] J. Cardy, *Ann. Phys. (Amsterdam)* **318**, 81 (2005).
- [6] M. Bauer and D. Bernard, *Phys. Rep.* **432**, 115 (2006).
- [7] M. Henkel and D. Karevski, *Conformal Invariance: An Introduction to Loops, Interfaces and Stochastic Loewner Evolution*, Lecture Notes in Physics (Springer Berlin Heidelberg, 2012).
- [8] D. Bernard, G. Boffetta, A. Celani, and G. Falkovich, *Nat. Phys.* **2**, 124 (2006).
- [9] L. Puggioni, A. G. Kritsuk, S. Musacchio, and G. Boffetta, *Phys. Rev. E* **102**, 023107 (2020).
- [10] D. Bernard, G. Boffetta, A. Celani, and G. Falkovich, *Phys. Rev. Lett.* **98**, 024501 (2007).
- [11] J. P. Keating, J. Marklof, and I. G. Williams, *Phys. Rev. Lett.* **97**, 034101 (2006).
- [12] E. Bogomolny, R. Dubertrand, and C. Schmit, *J. Phys. A* **40**, 381 (2007).
- [13] C. Amoruso, A. K. Hartmann, M. B. Hastings, and M. A. Moore, *Phys. Rev. Lett.* **97**, 267202 (2006).
- [14] D. Bernard, P. Le Doussal, and A. A. Middleton, *Phys. Rev. B* **76**, 020403(R) (2007).
- [15] G. Boffetta, A. Celani, D. Dezzani, and A. Seminara, *Geophys. Res. Lett.* **35**, L03615 (2008).
- [16] A. A. Saberi, M. A. Rajabpour, and S. Rouhani, *Phys. Rev. Lett.* **100**, 044504 (2008).
- [17] A. A. Saberi, M. D. Niry, S. M. Fazeli, M. R. Rahimi Tabar, and S. Rouhani, *Phys. Rev. E* **77**, 051607 (2008).
- [18] A. A. Saberi, S. Moghimi-Araghi, H. Dashti-Naserabadi, and S. Rouhani, *Phys. Rev. E* **79**, 031121 (2009).
- [19] G. Falkovich and S. Musacchio, [arXiv:1012.3868](https://arxiv.org/abs/1012.3868).
- [20] S. Thalabard, D. Rosenberg, A. Pouquet, and P. D. Mininni, *Phys. Rev. Lett.* **106**, 204503 (2011).
- [21] E. Daryaei, N. A. M. Araujo, K. J. Schrenk, S. Rouhani, and H. J. Herrmann, *Phys. Rev. Lett.* **109**, 218701 (2012).
- [22] I. Giordanelli, N. Posé, M. Mendoza, and H. J. Herrmann, *Sci. Rep.* **6**, 22949 (2016).
- [23] N. Posé, K. J. Schrenk, N. A. M. Araújo, and H. J. Herrmann, *Sci. Rep.* **4**, 5495 (2014).
- [24] C. P. De Castro, M. Luković, G. Pompanin, R. F. S. Andrade, and H. J. Herrmann, *Sci. Rep.* **8**, 5286 (2018).
- [25] G. Falkovich, *J. Phys. A* **42**, 123001 (2009).
- [26] V. Zakharov, V. Lvov, and G. Falkovich, *Kolmogorov Spectra of Turbulence*, Kolmogorov Spectra of Turbulence I: Wave Turbulence Vol. 1 (Springer-Verlag, Berlin, 1992).
- [27] S. Nazarenko, *Wave Turbulence*, Lecture Notes in Physics (Springer Berlin Heidelberg, 2011).
- [28] V. Shrira and S. Nazarenko, *Advances In Wave Turbulence*, World Scientific Series On Nonlinear Science Series A (World Scientific Publishing Company, Singapore, 2013).
- [29] S. Galtier, *Physics of Wave Turbulence* (Cambridge University Press, Cambridge, 2022).
- [30] D. Chelkak, H. Duminil-Copin, C. Hongler, A. Kemppainen, and S. Smirnov, *C. R. Math.* **352**, 157 (2014).
- [31] E. Falcon, S. Fauve, and C. Laroche, *Phys. Rev. Lett.* **98**, 154501 (2007).
- [32] E. Herbert, N. Mordant, and E. Falcon, *Phys. Rev. Lett.* **105**, 144502 (2010).
- [33] P. Cobelli, A. Prasadka, P. Petitjeans, G. Lagubeau, V. Pagneux, and A. Maurel, *Phys. Rev. Lett.* **107**, 214503 (2011).
- [34] E. Falcon and N. Mordant, *Annu. Rev. Fluid Mech.* **54**, 1 (2022).

- [35] W. B. Wright, R. Budakian, and S. J. Putterman, *Phys. Rev. Lett.* **76**, 4528 (1996).
- [36] W. B. Wright, R. Budakian, D. J. Pine, and S. J. Putterman, *Science* **278**, 1609 (1997).
- [37] See Supplemental Material at <http://link.aps.org/supplemental/10.1103/PhysRevLett.132.094001> for more information.
- [38] A. Ishimaru, *Wave Propagation and Scattering in Random Media* (Elsevier Science, New York, 1978).
- [39] M. Berhanu and E. Falcon, *Phys. Rev. E* **87**, 033003 (2013).
- [40] E. Henry, P. Alstrøm, and M. T. Levinsen, *Europhys. Lett.* **52**, 27 (2000).
- [41] H. Xia, T. Maimbourg, H. Punzmann, and M. Shats, *Phys. Rev. Lett.* **109**, 114502 (2012).
- [42] N. Francois, H. Xia, H. Punzmann, S. Ramsden, and M. Shats, *Phys. Rev. X* **4**, 021021 (2014).
- [43] N. Francois, H. Xia, H. Punzmann, P. W. Fontana, and M. Shats, *Nat. Commun.* **8**, 14325 (2017).
- [44] J. D. Hunter, *Comput. Sci. Eng.* **9**, 90 (2007).
- [45] B. Mandelbrot, *Science* **156**, 636 (1967); *The Fractal Geometry of Nature* (W. H. Freeman and Co., New York, 1983).
- [46] T. Kennedy, *J. Stat. Phys.* **137**, 839 (2009).
- [47] J. Foster, T. Lyons, and V. Margarint, *J. Stat. Phys.* **189**, 18 (2022).
- [48] K. Löwner, *Math. Ann.* **89**, 103 (1923).
- [49] O. Schramm, *Electron. Commun. Probab.* **6**, 115 (2001).
- [50] D. E. Marshall and S. Rohde, *SIAM J. Numer. Anal.* **45**, 2577 (2007).
- [51] T. Kennedy, *J. Stat. Phys.* **128**, 1125 (2007).
- [52] T. Kennedy, *J. Stat. Phys.* **131**, 803 (2008).
- [53] G. F. Lawler, An introduction to the stochastic Loewner evolution, in *Random Walks and Geometry*, edited by V. A. Kaimanovich (De Gruyter, Berlin, New York, 2004), pp. 261–294.
- [54] V. Beffara, *Ann. Probab.* **36**, 1421 (2008).